Available online at BCREC website: https://bcrec.id

Bulletin of Chemical Reaction Engineering & Catalysis, 16 (3) 2021, 641-650

Research Article

Ni Nanoparticles on Reducible Metal Oxides (Sm_2O_3, CeO_2, ZnO) as Catalysts for CO_2 Methanation

Athirah Ayub, Hasliza Bahruji*, Abdul Hanif Mahadi

Centre for Advanced Material and Energy Sciences, Universiti Brunei Darussalam, Jalan Tungku Link, BE1410, Brunei Darussalam.

Received: 4th May 2021; Revised: 6th July 2021; Accepted: 6th July 2021
Available online: 8th July 2021; Published regularly: September 2021

Abstract

The activity of reducible metal oxide Sm_2O_3, CeO_2, and ZnO as Ni nanoparticles support was investigated for CO_2 methanation reaction. CO_2 methanation was carried out between 200 °C to 450 °C with the optimum catalytic activity was observed at 450 °C. The reducibility of the catalysts has been comparatively studied using H_2-Temperature Reduction Temperature (TPR) method. The H_2-TPR analysis also elucidated the formation of surface oxygen vacancies at temperature above 600 °C for $5Ni/Sm_2O_3$ and $5Ni/CeO_2$. The Sm_2O_3 showed superior activity than CeO_2 presumably due to the transition of the crystalline phases under reducing environment. However, the formation of NiZn alloy in 5Ni/ZnO reduced the ability of Ni to catalyze methanation reaction. A highly dispersed Ni on Sm_2O_3 created a large metal/support interfacial interaction to give 69% of CO_2 conversion with 100% selectivity at 450 °C. The $5Ni/Sm_2O_3$ exhibited superior catalytic performances with an apparent phase transition from cubic to a mixture of cubic and monoclinic phases over a long reaction, presumably responsible for the enhanced conversion after 10 h of reaction.

Keywords: Ni nanoparticles; metal oxides (Sm_2O_3, CeO_2, ZnO); CO_2; methanation

How to Cite: A. Ayub, H. Bahruji, A.H. Mahadi (2021). Ni Nanoparticles on Reducible Metal Oxides (Sm_2O_3, CeO_2, ZnO) as Catalysts for CO_2 Methanation. *Bulletin of Chemical Reaction Engineering & Catalysis*, 16(3), 641-650 (doi:10.9767/bcrec.16.3.10948.641-650)

Permalink/DOI: https://doi.org/10.9767/bcrec.16.3.10948.641-650

1. Introduction

Utilization of CO_2 as carbon feedstock via the conversion to methane has been identified as a sustainable technology to produce renewable energy [1]. CO_2 reduced under H_2 gas at atmospheric pressure to form methane in the presence of metal catalysts. In order to overcome the thermodynamic of the reaction, investigation is carried out to synthesis catalysts with high methanation potential [2]. Modification of metal oxide with metal nanoparticles increases the hydrogenation potential [3] and the surface oxygen vacancy [4]. Ceria (CeO_2) is generally used as support for CO_2 methanation, and as a promoter to enhance surface oxygen vacancy of the catalysts [5,6]. In order to design active catalysts for the reaction, several parameters are modified for example Ni dispersion [7], Ni reducibility [8] and CO_2 adsorption capacity [9]. On the non-reducible support such as Al_2O_3 and zeolite, Ce was shown to improve metal-support interaction and reducibility of the catalysts [10]. Promoters such as K and Ba are added to improve the reducibility of Cu by covering the surface of Al_2O_3 support that allowed Cu to be easily accessible [11]. The reducibility of metal oxide provides the

* Corresponding Author.
Email: hasliza.bahruji@ubd.edu.bn (H. Bahruji)

flexibility of the catalyst surface during CO_2 methanation which mostly was associated with the presence of surface defect [12]. Depending on the degree of reducibility, reducible metal oxide, such as CeO_2, decreases the CO coverage on Ru metal center, to ensure the dissociation of H_2 can occur for the generation of methane [13]. However, on a non-reducible metal oxide such Al_2O_3, the catalytic activity is largely correlated with the basicity of the catalyst [13].

The activity of CeO_2, Sm_2O_3, and ZnO as reducible oxides support will be investigated in improving Ni activity for CO_2 methanation. CeO_2 represented as among the mostly investigated metal oxide for CO_2 methanation reaction [14,15]. The oxidation states of cerium are interchangeable between 4+ and 3+, with the Ce^{3+} ions signified the presence of oxygen vacancies and the migration of sub-surface oxygen [16]. Rare-earth metal oxide Sm_2O_3 was reported as promoter for CO_2 methanation that exhibited high activity, stability and coke resistance when incorporated with Ni/SBA-15 catalysts [17]. As a support, the Sm_2O_3 showed high activity when loaded with 39% of Ni to give ~71% of CO_2 conversion to methane at 300 °C [18]. ZnO is another interesting reducible metal oxide as catalyst support, however its reducibility is associated with the ability to transfer the charge to fill the *d*-band of metal for the formation of metal alloy [19,20]. ZnO was reported as active support for CO_2 hydrogenation to methanol when impregnated with Pd due to the formation of Pd-Zn alloy that can stabilize formate intermediate [21–23]. In this study, the catalytic activity of Ni supported on reducible metal oxides, CeO_2, Sm_2O_3, and ZnO were investigated for CO_2 methanation at different reaction temperatures. Reducible metal oxide has the ability to release electron under reducing environment for dissociation of C–O bond, however the reducible support can also change the structural and electronic properties of Ni. Due to the reducibility of these support, the presence of continuous hydrogen gas as reducing agent in CO_2 methanation also modified the structure of the catalysts. This study elucidate the changes on Ni nanoparticles activity when exists in metallic and alloy states upon impregnation on reducible support. Comparative H_2–TPR analysis is used to provide understanding on the dispersion and the reducibility of Ni, meanwhile X-ray Diffraction (XRD), N_2 adsorption, and Transmission Electron Microscopy (TEM) are employed for structural and morphology analysis.

2. Materials and Methods

2.1 Preparation of the Catalysts

All the catalysts were prepared using wetness impregnation method. $Ni(NO_3)_2$ at 5% of weight loading was dissolved in 10 mL of water. The amount of Ni loading was kept at 5% for all catalysts. The $Ni(NO_3)_2$ solution was added into metal oxide supports, CeO_2, Sm_2O_3, and ZnO, and stirred for 3 h at 60 °C to ensure thorough dispersion. The catalysts were dried at 200 °C for 2 h and then calcined at 500 °C for 3 h in air with a heating rate of 10 °C/min.

2.2 Characterization of the Catalysts

X-ray powder diffraction (Shimadzu XRD-700 X-ray Diffractometer) was carried out to analyze the crystalline structure of the catalysts by utilizing Cu-Kα radiation at λ = 1.54 Å, with operating conditions of 60 kV and 50 mA. The scanning angle range, 2θ, was 10–70° with a scan rate of 2°/min. The crystalline structure size was calculated using Scherrer's equation (Equation (1)).

$$D = \frac{k\lambda}{\beta \cos\theta} \quad (1)$$

where D is the crystallite size (nm), λ is the wavelength of x-ray (1.54 Å), θ is the peak position (radians), k is Scherrer constant and β is the FWHM (radians).

Surface area, average pore volume and pore diameter of the catalysts were determined by N_2 adsorption at 77 K (Micromeritics ASAP 2020). The samples were degassed under carbon degassing conditions for 2 h at 300 °C. Brunauer-Emmett-Teller (BET) equation was used to calculate the catalysts' surface area and Barret-Joyner-Halenda (BJH) equation for pore volume and diameter calculation.

H_2 Temperature-Programmed Reduction (ChemBET Pulsar TPR/TPD, equipped with TCD) was performed to study the catalysts' reducibility of NiO species on the catalyst surface. Catalysts undergone pre-treatment in N_2 stream with flow of 75 mL/min at 100 °C for 1 h and later cooled down to 40 °C in the same gas stream. Catalysts were later heated to 900 °C with a heating rate of 10 °C/min in a $5\%H_2/N_2$ gas mixture with a flow rate of 75 ml/min.

2.3 Catalytic Testing

CO_2 methanation reaction was conducted in a stainless-steel plug flow reactor at atmospheric pressure and reaction temperature

ranging from 200 to 450 °C. 0.5 g of catalyst was placed in a tubular fixed bed reactor and reduced in situ with H_2 gas (99.9%) with flow rate of 20 mL/min at 450 °C for 3 h. The catalysts were cooled down to room temperature and $CO_2/H_2/N_2$ (15%/60%/25%) gases at 20 ml/min were flowed in the reactor for catalytic reaction. The gas effluent from reactor was analyzed by GC (Shimadzu GC-2014) after 1h. Reaction temperature was increased by 50 °C every hour and data were recorded. CO_2 conversion (Equation (2)), CH_4 (Equation (3)) and CO selectivity (Equation (4)), and CH_4 yield (Equation (5)) were calculated as follows:

$$x_{CO_2} = \left[\frac{m_{CH_4} + m_{CO}}{m_{CH_4} + m_{CO_2} + m_{CO}}\right] \times 100\% \quad (2)$$

$$S_{CH_4} = \left[\frac{m_{CH_4}}{m_{CH_4} + m_{CO}}\right] \times 100\% \quad (3)$$

$$S_{CO} = \left[\frac{m_{CO}}{m_{CH_4} + m_{CO}}\right] \times 100\% \quad (4)$$

$$Y_{CH_4} = x_{CO_2} \times S_{CH_4} \quad (5)$$

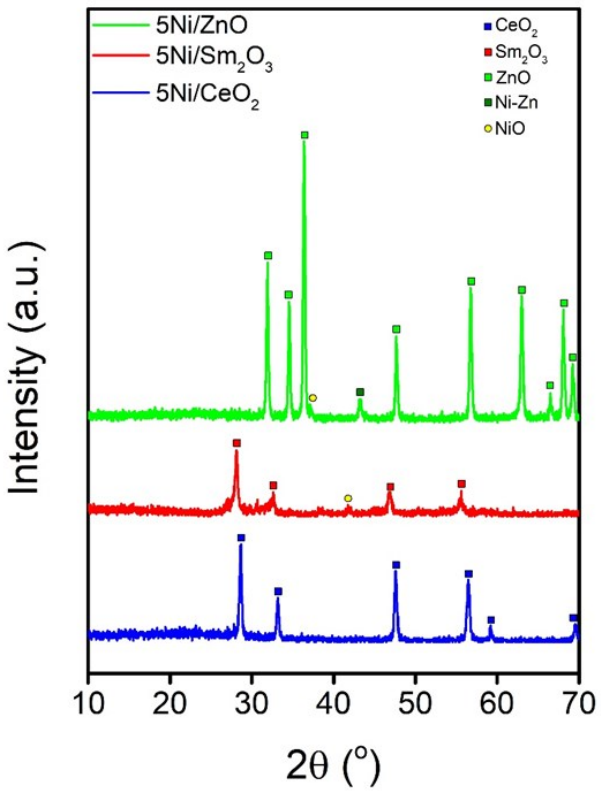

Figure 1. XRD patterns of $5Ni/CeO_2$, $5Ni/Sm_2O_3$ and 5Ni/ZnO after calcination at 500 °C and reduction at 450 °C.

Where x_{CO2}(%) is the CO_2 conversion, S_{CH4}(%) is the CH_4 selectivity, S_{CO}(%) is the CO selectivity, Y_{CH4}(%) is the CH_4 yield, and m is the number of moles of the gases.

3. Results and Discussion

3.1 XRD Analysis

Figure 1 showed the XRD analysis of $5Ni/CeO_2$, $5Ni/Sm_2O_3$, and 5Ni/ZnO after calcination in air at 500 °C and reduction in H_2 for 3 h at 400 °C. For $5Ni/CeO_2$, the characteristic peaks of CeO_2 were observed at 2θ = 28.6°, 33.1°, 47.5°, 56.4°, 59.2°, and 69.4° (JCPDS 043-1002). For $5Ni/Sm_2O_3$, the peaks assigned to Sm_2O_3 cubic crystalline phases were observed at 2θ = 28.2°, 32.7°, 46.9°, and 55.6° (JCPDS 043-1029) [15]. For 5Ni/ZnO, the characteristic peaks of ZnO were observed at 2θ= 31.9°, 34.5°, 36.3°, 47.5°, 56.7°, 62.9°, 66.4°, 68.0°, and 69.2° (JCPDS 036-1451). Small NiO peaks were observed in Ni/Sm_2O_3 at 2θ = 37.4° and 42.0°, corresponding to the NiO nanoparticles with estimated sizes of ~1.2 nm. In the $5Ni/CeO_2$, no peak associated with NiO was observed that may be due to the formation of highly disperse Ni nanoparticles [24]. The additional peak was observed at 2θ = 23.9° on 5Ni/ZnO catalyst which indicated the formation of Ni-Zn alloy.

3.2 N_2 Adsorption-Desorption Analysis

N_2 analysis was carried out to investigate the textural properties of the catalysts. Figure 2 presented the N_2 adsorption-desorption isotherms and pore size distributions of $5Ni/Sm_2O_3$, 5Ni/ZnO, and $5Ni/CeO_2$ after calcination at 500 °C for 3 h. Based on the IUPAC isotherm classification, all the catalysts displayed Type III isotherm, which is a typical feature of a non-porous material [25]. $5Ni/Sm_2O_3$ and $5Ni/CeO_2$ showed the presence of H3-hysteresis loop at high *P*/*P*o that suggested the formation porous structure [26]. The Type H3 loop at high P/Po was produced from the adsorption of multi-layer metastability and delayed capillary condensation which occurs in slit-shaped macropores or non-rigid aggregates of plate-like particles resulted from a low level of pore curvature and flexibility of the aggregate structure [26]. Table 1 summarized the textural properties of the catalysts calculated using BET equation. The $5Ni/CeO_2$ showed the highest surface area (15 m^2/g) followed with 5Ni/ZnO (13 m^2/g) and $5Ni/Sm_2O_3$ (9 m^2/g). The plot of pore size distribution showed the presence of pores at ~21 nm on $5Ni/TiO_2$ catalysts

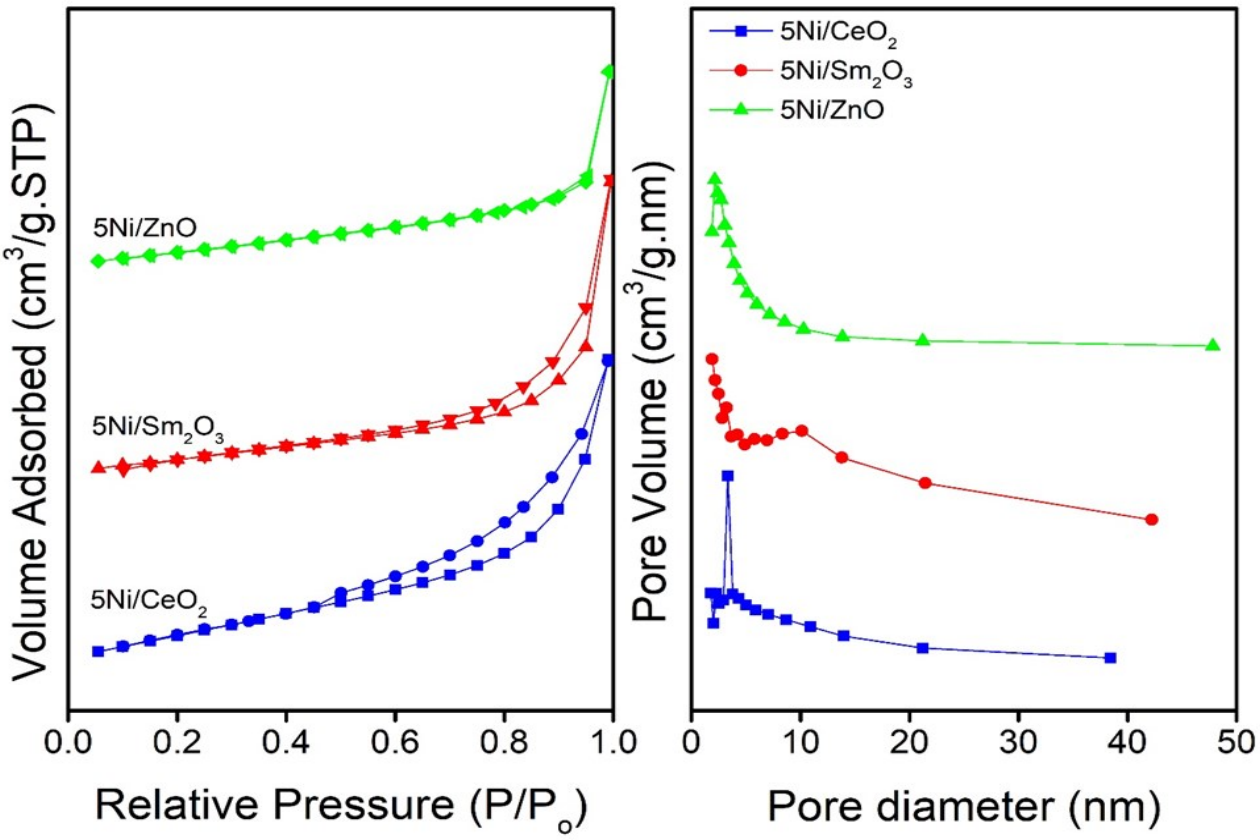

Figure 2. (a) N_2 adsorption-desorption isotherm plot and (b) pore size distribution for $5Ni/CeO_2$, $5Ni/Sm_2O_3$, and 5Ni/ZnO after calcination at 500 °C.

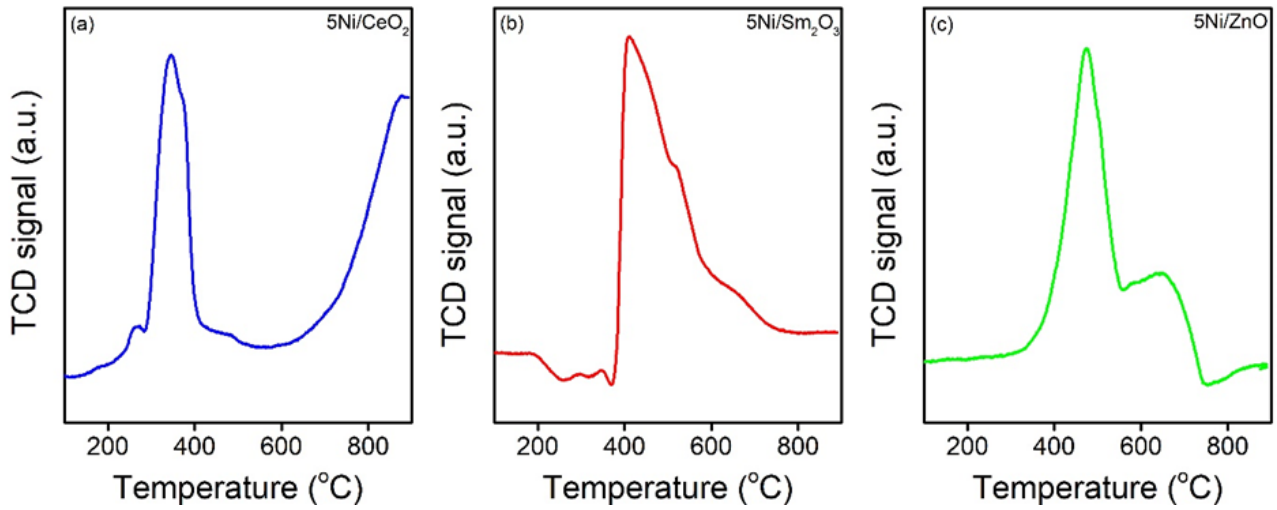

Figure 3. H_2-TPR profiles of $5Ni/CeO_2$, $5Ni/Sm_2O_3$ and 5Ni/ZnO after calcination at 500 °C.

Table 1. Physical and textural properties, and CO_2 conversion of Ni on CeO_2, Sm_2O_3, and ZnO. Reaction temperature: 450 °C.

Catalyst	S_{BET} (m^2/g)	Pore Volume (cm^3/g)	Pore Size (nm)	Ni sites (mmol/g)	X_{CO2} (%)	S_{CH4} (%)
$5Ni/CeO_2$	15	0.0431	2.3, 3.3	6.8	67.6	99.5
$5Ni/Sm_2O_3$	9	0.0419	2.0, 11.0	18.5	69.3	100
5Ni/ZnO	13	0.0421	2.1	5.2	26.6	99.5

presumably due to the formation of interparticle mesopores.

3.3 H_2–TPR Analysis

Temperature Programmed Reduction (TPR) was carried out on the catalysts to investigate the reducibility and the dispersion of Ni particles (Figure 3). In general, the reducibility of Ni catalyst was determined based on the position of the reduction peak at 250–500 °C due to reduction of NiO to metallic Ni. 5Ni/ZnO showed the first reduction peak centered at 470 °C and was accompanied with a broad reduction peak between 550–700 °C. The first reduction peak was associated with the reduction of α-type NiO species, generally reduced at low-temperature region (300–500 °C) [27,28]. Meanwhile, the broad reduction peak observed between 550–700 °C was due to the segregation of ZnO to Ni-Zn alloy [29]. The presence of Ni-Zn alloy was evidenced from the XRD analysis (Figure 1). The 5Ni/CeO_2 showed the first reduction peak appeared at 350 °C and a small peak at 290 °C. The multiple H_2 consumption peaks indicated the differences between interaction of NiO species with the metal oxide support [30]. Increasing the temperature to 900 °C showed a broad reduction peak started at 600 °C and was continuously increased at temperature above 900 °C. At temperature above 600 °C, the oxygen in ceria surface was removed when reacted with H_2, releasing water and creating surface oxygen vacancies [30]. The vacancies were formed from the reduction of Ce^{4+} to Ce^{3+} under H_2 flow. The 5Ni/Sm_2O_3 showed a broad reduction profile of NiO with the peak centered at 411 °C. Sm_2O_3 was reduced at temperature above 700 °C due to reduction of Sm_2O_3 to SmO in the absence of Ni [31]. It is suggested that the reduction peak of Sm_2O_3 was reduced to temperature below 700 °C due to the H_2 spillover from Ni. The reduction peak of NiO was overlapped with the reduction peak of Sm_2O_3 thus produced a broad TPR profile on Ni/Sm_2O_3. The Sm_2O_3 was reduced at temperature below 700 °C, significantly lower than the reduction of CeO_2 which was occurred at temperature above 700 °C. The results implied the tendency of Sm_2O_3 to generate oxygen vacancies under H_2 flow was higher than CeO_2.

3.4 TEM-EDX Analysis

TEM analysis was carried out to determine the morphology of 5Ni/Sm_2O_3 catalyst and to acquire the average diameter of Ni particles. 5Ni/Sm_2O_3 was calcined in air and reduced in hydrogen gas prior to the TEM analysis. Figure 4 showed the representative TEM image of 5Ni/Sm_2O_3 with its corresponding EDX analysis. Ni was well distributed on Sm_2O_3 surface evidenced from the formation of spherical shapes particles as shown in a small red circle. The particle size of Ni nanoparticles was analyzed using ImageJ and the average diameter was determined at ~2 nm. The EDX elemental analysis of 5Ni/Sm_2O_3 further confirmed the presence of Ni at ~5% loading. The elemental mapping also indicated the homogeneous dispersion of Ni on Sm_2O_3.

3.5 Catalytic Activity

CO_2 methanation was carried out 200–450 °C at atmospheric pressure (Equation (6)). Prior to the reaction, the catalyst was reduced in-situ at 450 °C under H_2 flow for 3 h. Table 1

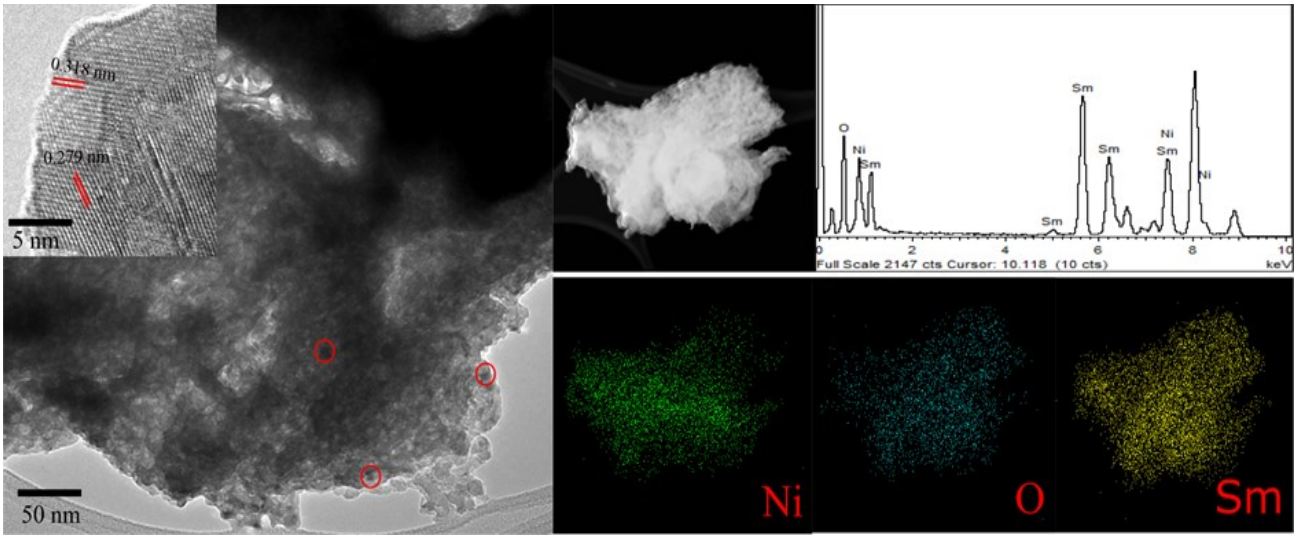

Figure 4. HRTEM-EDX analysis of 5Ni/Sm_2O_3 catalyst.

summarized the physicochemical properties and the catalytic performances of all the catalysts at 450 °C. The 5Ni/CeO_2 showed 67.6% of CO_2 conversion with 100% selectivity towards methane. When Ni was impregnated onto Sm_2O_3, the conversion of CO_2 was slightly increased to 69.3% at 100% selectivity to methane. If the reaction was carried out using 5Ni/ZnO, the CO_2 conversion was observed at 26.6% with 99.5% selectivity to methane. Unlike CeO_2 and Sm_2O_3, ZnO showed a relatively low catalytic conversion presumably due to the formation of Ni-Zn alloy on the catalysts that reduced the activity of Ni towards methanation reaction. In CO_2 methanation reaction, it was reported that Ni must be in its zero oxidation states to catalyze hydrogen dissociation [32]. The use of ZnO as support, formed Ni-Zn alloy that changed the electronic properties of Ni. The charge transfer from Ni to Zn transformed the metallic Ni with zero oxidation state to be partially positive charged NiZn [33]. The NiZn promoted the formation of CO_2 hydrogenation to C_2 products due to further hydrogenation of formate intermediates [34]. The formation of Ni_5Ga_3 alloy was also observed on Ga_2O_3 support, responsible for enhanced methanol formation from CO_2 [35]. There is also possibility that NiZn alloy further catalyzed the resulting methane into CO via dry reforming reaction [36]. Therefore, the efficiency of Ni alloy in 5Ni/ZnO catalyst for methanation reaction was reduced to give only 26.6% of CO_2 conversion at 450 °C, with CO was also determined as the result of reverse water gas shift reaction (Equation (7)).

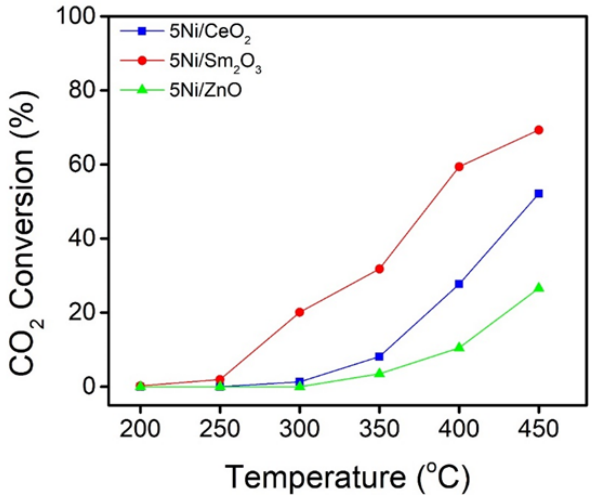

Figure 5. CO_2 methanation on 5Ni/Sm_2O_3, 5Ni/CeO_2 and 5Ni/ZnO at temperatures between 200 °C to 450 °C.

$$CO_{2\,(g)} + 4H_{2\,(g)} \leftrightarrow CH_{4\,(g)} + 2H_2O_{\,(g)}$$
$$\Delta H_{298K} = -165 \text{ kJ/mol} \quad (6)$$

$$CO_{2\,(g)} + H_{2\,(g)} \leftrightarrow CO_{\,(g)} + 2H_2O_{\,(g)}$$
$$\Delta H_{298K} = -41.2 \text{ kJ/mol} \quad (7)$$

CO_2 methanation was carried out further at different reaction temperatures to study the performance of Ni on reducible metal supports at low temperatures (Figure 5, Table 2). All the catalysts were seen to be inactive at both 200 °C and 250 °C but methane formation was starting to observe at 300 °C, in exception for 5Ni/ZnO catalyst. Evidently, 5Ni/Sm_2O_3 showed the highest activity at low temperatures with the CO_2 conversion at 300 °C was measured at 20.1%. The reactivity was then followed by 5Ni/CeO_2 and 5Ni/ZnO. At the variation of reaction temperatures, both 5Ni/CeO_2 and 5Ni/Sm_2O_3 displayed 100% CH_4 selectivity. However, for 5Ni/ZnO, as reaction temperature increased over 350 °C, 5Ni/ZnO only demonstrated 73.7% selectivity towards methane, with CO was produced as a side product. The production of methane was enhanced at 450 °C, to give 87% selectivity with 26.6% conversion of CO_2.

3.6 Stability Studies of Ni/Sm_2O_3

To further investigate the stability of 5Ni/Sm_2O_3, catalytic reaction was carried out for 28 h at 300 °C. Figure 6(a) showed the CO_2 conversion was measured at 20% at the first 60

Table 2. Catalytic activity of Ni on CeO_2, Sm_2O_3 and ZnO at different reaction temperatures.

Temperature (°C)	CO_2 Conversion (%)			CH_4 Selectivity (%)		
	5Ni/CeO_2	5Ni/Sm_2O_3	5Ni/ZnO	5Ni/CeO_2	5Ni/Sm_2O_3	5Ni/ZnO
200	0	0.2	0	0	100	0
250	0	1.9	0	0	100	0
300	1.3	20.1	0	100	100	0
350	8.1	31.8	3.5	100	100	73.7
400	27.7	59.4	10.5	100	100	87.0
450	52.1	69.3	26.6	99.5	100	94.7

min into the reaction. The conversion was significantly improved after 2 h to give ~32% conversion and the conversion was stable for the next 10 h of reaction. It is interesting to note that CO_2 conversion was improved to ~51% at 15 h of reaction and the conversion was maintained until 28 h. The XRD of the catalysts after 5 h and 28 h were analyzed to determine the structural changes of $5Ni/Sm_2O_3$ (Figure 6(b)). XRD analysis of $5Ni/Sm_2O_3$ following 5 h reaction showed no significant differences on the structure of the catalysts. All the peaks corresponded to the Sm_2O_3 in the cubic crystal structure were visible, according to JCPDS 043-1029. When the XRD analysis was carried out on $5Ni/Sm_2O_3$ after 28 h catalytic reaction, the new peak corresponded to Ni metal at 2θ = 47° was gained significant enhancement in intensity suggesting the NiO nanoparticles was sintered to form large Ni crystallites. Two new peaks corresponded to Sm_2O_3 with monoclinic phase were observed at 27° and 39.8° (JCPDS card no 042-1464) [37]. The transition of Sm_2O_3 phase from cubic to monoclinic implied the increase of catalytic activity after 10 h of reaction maybe due to the formation of more active Sm_2O_3 sites due to the prolonged reduction under $CO_2/H_2/N_2$ mixed gas during reaction. Cubic phase was characterized by a larger distance between the ions with isometric and higher entropy, meanwhile monoclinic structure had a shorter distance between the ions with a minimal bond energy [38]. Although the transition between cubic to monoclinic phase in Sm_2O_3 was reported at high temperatures ~1000 °C [39], there was a possibility that impregnation with Ni and annealing under H_2 gas reduced the temperature for the phase transformation. HRTEM analysis of Ni/Sm_2O_3 further confirmed the presence of cubic and monoclinic phases (Figure 4). The distances between planes were measured to be 0.318 nm which corresponded to the (222) planes of cubic phase Sm_2O_3 [31], meanwhile the monoclinic phase was identified with the shorten lattice spacing at 0.27 nm due to shorter distance between the ions with a minimal bond energy of the monoclinic phase [38].

The activity of Ni nanoparticles was significantly enhanced when Sm_2O_3 was used as support mainly due to the increase of Ni dispersion on Sm_2O_3. Despite the surface area of Sm_2O_3 was significantly lower than ZnO and CeO_2, the number of Ni active sites on $5Ni/Sm_2O_3$ were determined at 18.5 mmol/g, which were higher than $5Ni/CeO_2$ at 6.8 mmol/g and 5Ni/ZnO at 5.6 mmol/g. Apart from the dispersion, the reducibility of metal nanoparticles also played an important role during the catalytic reaction Surface oxygen vacancies improved the adsorption and dissociation of CO_2. The energy required for the formation of vacancies in reducible oxides was relatively low compared to the non-reducible metal oxide. The activity of

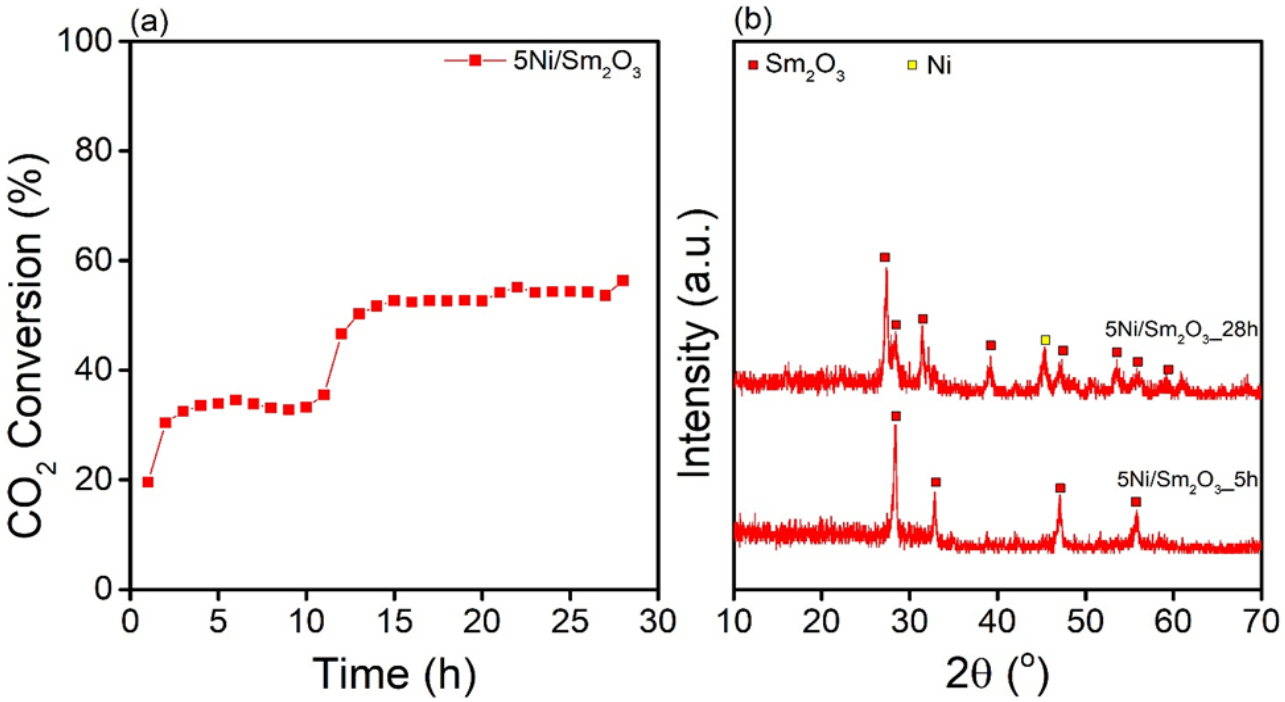

Figure 6. (a) CO_2 methanation of $5Ni/Sm_2O_3$ at 350 °C for 28 h; and (b) XRD analysis of post reaction $5Ni/Sm_2O_3$ catalyst after 5 h and after 28 h.

non-reducible oxide support was generally correlated with its basicity such as Al_2O_3 and zeolite [40]. The dissociated hydrogen on Ni, was spilled over to metal oxide support that can be used to form oxygen vacancies. The Sm_2O_3 and CeO_2 with 4+ oxidation states reduced to 3+ under hydrogen created oxygen vacancies to facilitate CO_2 adsorption. The proximity of Ni/support interfacial contact in $5Ni/Sm_2O_3$ compared to $5Ni/CeO_2$, due to the formation of highly dispersed metal nanoparticles, assisted the formation of oxygen vacancies. The highly dispersed Ni nanoparticles created a larger metal/support interaction, which was identified as the active sites for CO_2 methanation. Prolonged catalytic reaction further reduced the Sm_2O_3 via hydrogen spill over, which transformed the cubic phase into monoclinic phase. The combination of highly exposed metallic Ni and the continuous formation of oxygen vacancies on Sm_2O_3 created Ni-VO_x-Sm sites which were essential for CO_2 methanation [41].

4. Conclusion

The activity of $5Ni/Sm_2O_3$ was investigated as catalysts for methanation reaction and compared to another reducible oxide supports CeO_2 and ZnO. The importance of metallic Ni to catalyze methanation was further consolidated by the non-reactivity of 5Ni/ZnO catalysts due to the formation of Ni-Zn alloy. Ni was highly dispersed on Sm_2O_3 thus created a high interfacial contact for efficient formation of oxygen vacancies during catalytic reaction. The enhancement of CO_2 conversion after 10 h of reaction implied the formation of oxygen vacancies were continuously formed during the reaction, resulting in the transition of Sm_2O_3 crystal phase from cubic to monoclinic.

Acknowledgement

Authors would like to acknowledge Universiti Brunei Darussalam Research Grant UBD/RSCH/URC/RG(b)/2019/012 for funding of the project.

References

[1] Su, X., Xu, J., Liang, B., Duan, H., Hou, B., Huang, Y. (2016). Catalytic carbon dioxide hydrogenation to methane: A review of recent studies. *Journal of Energy Chemistry*, 25(4), 553–565. DOI: 10.1016/j.jechem.2016.03.009

[2] Boggula, R.R., Fischer, D., Casaretto, R., Born, J. (2020). Methanation potential: Suitable catalyst and optimized process conditions for upgrading biogas to reach gas grid requirements. *Biomass and Bioenergy*, 133, 105447. DOI: 10.1016/j.biombioe.2019.105447

[3] Garbarino, G., Riani, P., Magistri, L., Busca, G. (2014). A study of the methanation of carbon dioxide on Ni/Al_2O_3 catalysts at atmospheric pressure. *International Journal of Hydrogen Energy*, 39(22), 11557–11565. DOI: 10.1016/j.ijhydene.2014.05.111

[4] Everett, O.E., Zonetti, P.C., Alves, O.C., de Avillez, R.R., Appel, L.G. (2020). The role of oxygen vacancies in the CO_2 methanation employing Ni/ZrO_2 doped with Ca. *International Journal of Hydrogen Energy*, 45(11), 6352–6359. DOI: 10.1016/j.ijhydene.2019.12.140

[5] Makdee, A., Chanapattharapol, K.C., Kidkhunthod, P., Poo-arporn, Y., Ohno, T. (2020). The role of Ce addition in catalytic activity enhancement of TiO_2-supported Ni for CO_2 methanation reaction. *RSC Advances*, 10(45), 26952–26971. DOI: 10.1039/D0RA04934D

[6] Gac, W., Zawadzki, W., Rotko, M., Słowik, G., Greluk, M. (2019). CO_2 Methanation in the Presence of Ce-Promoted Alumina Supported Nickel Catalysts: H_2S Deactivation Studies. *Topics in Catalysis*, 62(5), 524–534. DOI: 10.1007/s11244-019-01148-3

[7] Zeng, L., Wang, Y., Li, Z., Song, Y., Zhang, J., Wang, J., He, X., Wang, C., Lin, W. (2020). Highly Dispersed Ni Catalyst on Metal–Organic Framework-Derived Porous Hydrous Zirconia for CO_2 Methanation. *ACS Applied Materials & Interfaces*, 12(15), 17436–17442. DOI: 10.1021/acsami.9b23277

[8] Guilera, J., del Valle, J., Alarcón, A., Díaz, J. A., Andreu, T. (2019). Metal-oxide promoted Ni/Al_2O_3 as CO_2 methanation micro-size catalysts. *Journal of CO_2 Utilization*, 30, 11–17. DOI: 10.1016/j.jcou.2019.01.003

[9] Le, M.C., Van, K.L., Nguyen, T.H.T., Nguyen, N.H. (2017). The Impact of Ce-Zr Addition on Nickel Dispersion and Catalytic Behavior for CO_2 Methanation of Ni/AC Catalyst at Low Temperature. *Journal of Chemistry*, 2017, 4361056. DOI: 10.1155/2017/4361056

[10] Daroughegi, R., Meshkani, F., Rezaei, M. (2021). Enhanced low-temperature activity of CO_2 methanation over ceria-promoted Ni-Al_2O_3 nanocatalyst. *Chemical Engineering Science*, 230, 116194. DOI: 10.1016/j.ces.2020.116194

[11] Bansode, A., Tidona, B., von Rohr, P.R., Urakawa, A. (2013). Impact of K and Ba promoters on CO_2 hydrogenation over Cu/Al_2O_3 catalysts at high pressure. *Catalysis Science & Technology*, 3(3), 767–778. DOI: 10.1039/C2CY20604H

[12] Takano, H., Shinomiya, H., Izumiya, K., Kumagai, N., Habazaki, H., Hashimoto, K. (2015). CO_2 methanation of Ni catalysts supported on tetragonal ZrO_2 doped with Ca^{2+} and Ni^{2+} ions. *International Journal of Hydrogen Energy*, 40(26), 8347–8355. DOI: 10.1016/j.ijhydene.2015.04.128

[13] Dreyer, J.A.H., Li, P., Zhang, L., Beh, G.K., Zhang, R., Sit, P.H.L., Teoh, W.Y. (2017). Influence of the oxide support reducibility on the CO_2 methanation over Ru-based catalysts. *Applied Catalysis B: Environmental*, 219, 715–726. DOI: 10.1016/j.apcatb.2017.08.011

[14] Atzori, L., Cutrufello, M.G., Meloni, D., Monaci, R., Cannas, C., Gazzoli, D., Sini, M.F., Deiana, P., Rombi, E. (2017). CO_2 methanation on hard-templated $NiOCeO_2$ mixed oxides. *International Journal of Hydrogen Energy*, 42(32), 20689–20702. DOI: 10.1016/j.ijhydene.2017.06.198

[15] Fukuhara, C., Hayakawa, K., Suzuki, Y., Kawasaki, W., Watanabe, R. (2017). A novel nickel-based structured catalyst for CO_2 methanation: A honeycomb-type Ni/CeO_2 catalyst to transform greenhouse gas into useful resources. *Applied Catalysis A: General*, 532, 12–18. DOI: 10.1016/j.apcata.2016.11.036

[16] Tok, A.I.Y., Du, S.W., Boey, F.Y.C., Chong, W.K. (2007). Hydrothermal synthesis and characterization of rare earth doped ceria nanoparticles. *Materials Science and Engineering: A*, 466(1), 223–229. DOI: 10.1016/j.msea.2007.02.083

[17] Taherian, Z., Yousefpour, M., Tajally, M., Khoshandam, B. (2017). A comparative study of ZrO_2, Y_2O_3 and Sm_2O_3 promoted Ni/SBA-15 catalysts for evaluation of CO_2/methane reforming performance. *International Journal of Hydrogen Energy*, 42(26), 16408–16420. DOI: 10.1016/j.ijhydene.2017.05.095

[18] Ilsemann, J., Sonström, A., Gesing, T.M., Anwander, R., Bäumer, M. (2019). Highly Active Sm_2O_3-Ni Xerogel Catalysts for CO_2 Methanation. *ChemCatChem*, 11(6), 1732–1741. DOI: 10.1002/cctc.201802049

[19] Brix, F., Desbuis, V., Piccolo, L., Gaudry, É. (2020). Tuning Adsorption Energies and Reaction Pathways by Alloying: PdZn versus Pd for CO_2 Hydrogenation to Methanol. *The Journal of Physical Chemistry Letters*, 11(18), 7672–7678. DOI: 10.1021/acs.jpclett.0c02011

[20] Ojelade, O.A., Zaman, S.F., Daous, M.A., Al-Zahrani, A.A., Malik, A.S., Driss, H., Shterk, G., Gascon, J. (2019). Optimizing Pd:Zn molar ratio in $PdZn/CeO_2$ for CO_2 hydrogenation to methanol. *Applied Catalysis A: General*, 584, 117185. DOI: 10.1016/j.apcata.2019.117185

[21] Bahruji, H., Armstrong, R.D., Ruiz Esquius, J., Jones, W., Bowker, M., Hutchings, G.J. (2018). Hydrogenation of CO_2 to dimethyl ether over Brønsted acidic PdZn catalysts. *Industrial & Engineering Chemistry Research*, 57(20), 6821–6829. DOI: 10.1021/acs.iecr.8b00230.

[22] Bahruji, H., Bowker, M., Jones, W., Hayward, J., Ruiz Esquius, J., Morgan, D.J., Hutchings, G.J. (2017). PdZn catalysts for CO_2 hydrogenation to methanol using chemical vapour impregnation (CVI). *Faraday Discussions*, 197(0), 309–324. DOI: 10.1039/C6FD00189K

[23] Bahruji, H., Esquius, J.R., Bowker, M., Hutchings, G., Armstrong, R.D., Jones, W. (2018). Solvent Free Synthesis of $PdZn/TiO_2$ Catalysts for the Hydrogenation of CO_2 to Methanol. *Topics in Catalysis*, 61(3-4), 144–153. DOI: 10.1007/s11244-018-0885-6

[24] Rui, N., Zhang, X., Zhang, F., Liu, Z., Cao, X., Xie, Z., Zou, R., Senanayake, S.D., Yang, Y., Rodriguez, J.A., Liu, C. (2021). Highly active Ni/CeO_2 catalyst for CO_2 methanation: Preparation and characterization. *Applied Catalysis B: Environmental*, 282, 119581. DOI: 10.1016/j.apcatb.2020.119581.

[25] Thommes, M., Kaneko, K., Neimark, A.V., Olivier, J.P., Rodriguez-Reinoso, F., Rouquerol, J., Sing, K.S.W. (2015). Physisorption of gases, with special reference to the evaluation of surface area and pore size distribution (IUPAC Technical Report). *Pure and Applied Chemistry*, 87(9-10), 1051–1069. DOI: 10.1515/pac-2014-1117

[26] Alothman, Z.A. (2012). A Review: Fundamental Aspects of Silicate Mesoporous Materials. *Materials*, 5(12), 2874–2902. DOI: 10.3390/ma5122874

[27] Dias, Y.R., Perez-Lopez, O.W. (2020). Carbon dioxide methanation over $Ni-Cu/SiO_2$ catalysts. *Energy Conversion and Management*, 203, 122214. DOI: 10.1016/j.enconman.2019.112214.

[28] Lv, C., Xu, L., Chen, M., Cui, Y., Wen, X., Wu, C., Yang, B., Wang, F., Miao, Z,. Hu, X., Shou, Q. (2020). Constructing highly dispersed Ni based catalysts supported on fibrous silica nanosphere for low-temperature CO_2 methanation. *Fuel*, 278, 118333. DOI: 10.1016/j.fuel.2020.118333.

[29] Qi, J., Hu, X. (2020). The loss of ZnO as the support for metal catalysts by H_2 reduction. *Physical Chemistry Chemical Physics*, 22(7), 3953–3958. DOI: 10.1039/c9cp06093f.

[30] Lee, J., Ryou, Y., Chan, X., Kim, T.J., Kim, D.H. (2016). How Pt Interacts with CeO2 under the Reducing and Oxidizing Environments at Elevated Temperature: The Origin

of Improved Thermal Stability of Pt/CeO_2 Compared to CeO_2. *The Journal of Physical Chemistry C*, 120(45), 25870–25879. DOI: 10.1021/acs.jpcc.6b08656

[31] Kang, J.-G., Min, B.-K., Sohn, Y. (2015). Synthesis and characterization of $Sm(OH)_3$ and Sm_2O_3 nanoroll sticks. *Journal of Materials Science*, 50(4), 1958–1964. DOI: 10.1007/s10853-014-8760-8

[32] Zhou, G., Liu, H., Cui, K., Jia, A., Hu, G., Jiao, Z., Liu, Y., Zhang, X. (2016). Role of surface Ni and Ce species of Ni/CeO_2 catalyst in CO2 methanation. *Applied Surface Science*, 383, 248–252. DOI: 10.1016/j.apsusc.2016.04.180

[33] Samanta, A., Das, S., Jana, S. (2020). Ultrasmall intermetallic NiZn nanoparticles: a non-precious metal catalyst for efficient electrocatalysis. *Nanoscale Advances*, 2(1), 417–424. DOI: 10.1039/C9NA00611G

[34] Zhang, XD., Liu, K., Fu, JW., Li, HM., Pan, H., Hu, JH., Liu, M. (2021). Pseudo-copper Ni-Zn alloy catalysts for carbon dioxide reduction to C_2 products. *Frontiers of Physics*, 16, 63500. DOI: 10.1007/s11467-021-1079-4

[35] Goyal, R., Lee, W.J., Sameer, S., Sarkar, B., Chiang, K., Bordoloi, A. (2020). CNx stabilized Ni-Ga nanoparticles for CO_2 hydrogenation: Role of preparation methods. Catalysis *Today*, 343, 48–55. DOI: 10.1016/j.cattod.2019.03.031

[36] Sokolov, S., Radnik, J., Schneider, M., Rodemerck, U. (2017). Low-temperature CO_2 reforming of methane over Ni supported on ZnAl mixed metal oxides. *International Journal of Hydrogen Energy*, 42(15), 9831–9839. DOI: 10.1016/j.ijhydene.2017.01.013.

[37] Sone, B.T., Manikandan, E., Gurib-Fakim, A., Maaza, M. (2015). Sm_2O_3 nanoparticles green synthesis via Callistemon viminalis' extract. *Journal of Alloys and Compounds*, 650, 357–362. DOI: 10.1016/j.jallcom.2015.07.272

[38] Barad, C., Kimmel, G., Hayun, H., Shamir, D., Hirshberg, K., Gelbstein, Y. (2020). Phase Stability of Nanocrystalline Grains of Rare-Earth Oxides (Sm_2O_3 and Eu_2O_3) Confined in Magnesia (MgO) Matrix. *Materials*, 13(9), 2201. DOI: 10.3390/ma13092201

[39] Zinkevich, M. (2007). Thermodynamics of rare earth sesquioxides. Progress *in Materials Science*, 52(4), 597–647. DOI: 10.1016/j.pmatsci.2006.09.002

[40] Sholeha, N.A., Jannah, L., Rohma, H.N., Widiastuti, N., Prasetyoko, D., Jalil, A.A., Bahruji, H. (2020). Synthesis of Zeolite NaY from Dealuminated Metakaolin as Ni Support for CO_2 Hydrogenation to Methane. *Clays and Clay Minerals*, 68(5), 513–523. https://doi.org/10.1007/s42860-020-00089-3

[41] Tada, S., Nagase, H., Fujiwara, N., Kikuchi, R. (2021). What Are the Best Active Sites for CO_2 Methanation over Ni/CeO_2?. *Energy & Fuels*, 35(6), 5241–5251. DOI: 10.1021/acs.energyfuels.0c04238